

Acidification of East Siberian Arctic Shelf waters through addition of freshwater and terrestrial carbon

Igor Semiletov^{1,2,3*}, Irina Pipko³, Örjan Gustafsson⁴, Leif G. Anderson⁵, Valentin Sergienko⁶, Svetlana Pugach³, Oleg Dudarev³, Alexander Charkin^{2,3}, Alexander Gukov⁷, Lisa Bröder⁴, August Andersson⁴, Eduard Spivak³ and Natalia Shakhova^{1,2}

Ocean acidification affects marine ecosystems and carbon cycling, and is considered a direct effect of anthropogenic carbon dioxide uptake from the atmosphere¹⁻³. Accumulation of atmospheric CO₂ in ocean surface waters is predicted to make the ocean twice as acidic by the end of this century⁴. The Arctic Ocean is particularly sensitive to ocean acidification because more CO₂ can dissolve in cold water^{5,6}. Here we present observations of the chemical and physical characteristics of East Siberian Arctic Shelf waters from 1999, 2000–2005, 2008 and 2011, and find extreme aragonite undersaturation that reflects acidity levels in excess of those projected in this region for 2100. Dissolved inorganic carbon isotopic data and Markov chain Monte Carlo simulations of water sources using salinity and $\delta^{18}\text{O}$ data suggest that the persistent acidification is driven by the degradation of terrestrial organic matter and discharge of Arctic river water with elevated CO₂ concentrations, rather than by uptake of atmospheric CO₂. We suggest that East Siberian Arctic Shelf waters may become more acidic if thawing permafrost leads to enhanced terrestrial organic carbon inputs and if freshwater additions continue to increase, which may affect their efficiency as a source of CO₂.

The calcium carbonate (CaCO₃) saturation state (Ω), both for aragonite (Ar, Ω_{Ar}) and for calcite, is expressed by the product of seawater CO₃²⁻ and Ca²⁺ concentrations relative to their stoichiometric solubility product at given temperature, salinity and pressure⁷. $\Omega > 1$ waters favour the formation of CaCO₃ shells and skeletons; $\Omega < 1$ waters are corrosive, causing CaCO₃ dissolution^{2,6}. Arctic Ocean Ω is lower than in other oceans because CO₂ is more soluble in colder waters⁴⁻⁶. Model studies suggest that open Arctic Ocean surface waters will be the first to become undersaturated ($\Omega < 1$) owing to increasing absorption of anthropogenic CO₂ from the atmosphere; this may happen within a decade^{7,8}. River discharge, ice melt, and anthropogenic pollution were shown to be contributing to ocean acidification (OA)⁹⁻¹¹. The present study synthesizes a decade of observations on the remote Arctic shelf seas aimed at exploring the extent to which natural Arctic system processes, such as degradation of terrestrial organic matter translocated

from thawed permafrost to the shelf waters^{12,13}, river discharge^{14,15}, and ice melt⁹, possibly amplified by regional warming¹⁶, may serve as coupled mechanisms to cause Ar undersaturation in the Arctic Ocean.

The extensive East Siberian Arctic Shelf, made up of the Laptev Sea, the East Siberian Sea, and the Russian part of the Chukchi Sea, which composes ~25% of the Arctic continental shelf, is believed to be a particularly vulnerable target area. The ESAS receives river discharge from four large Arctic rivers (Lena, Yana, Indigirka and Kolyma), which accumulate their waters from extensive permafrost-underlain watersheds. River discharge represents a great source of freshening¹¹; it also transports terrestrial organic carbon (terr-OC) to the shelves mobilized from extensive watersheds as a result of permafrost thawing^{13,17,18}. The ESAS near-shore system, including riverbanks, deltas and coastlines, includes thousands of km of Pleistocene ice complexes, composed of syncryogenic deposits with massive ice wedges (Supplementary Fig. 1a). This system is strongly affected by the warming that started in the early Holocene, when this shelf was inundated by sea water¹⁹. This long-lasting warming has caused the steep coastline to erode by several m yr⁻¹, releasing old organic matter held in permafrost into the shelf water^{20,21}. The massive amount of terr-OC delivered by rivers and coastal erosion is partly degraded and subjected to significant degradation during its residence in shelf water^{22,23}. Degradation of terr-OC was evident from levels of p_{CO_2} oversaturation²⁴⁻²⁶, removal fluxes of both terrestrial dissolved organic carbon²⁷ and particulate organic carbon²⁸, and from the molecular-specific shelf-wide $\delta^{13}\text{C}-\Delta^{14}\text{C}$ trends in particulate organic carbon¹³.

To investigate the state of Ω_{Ar} and elucidate factors controlling OA in two biogeochemical provinces of the ESAS²⁹ (Fig. 1a), we determined total alkalinity (TA), pH, dissolved inorganic carbon (DIC), p_{CO_2} , dissolved oxygen (O₂), apparent oxygen utilization (AOU), coloured dissolved organic matter (CDOM), suspended particulate matter (SPM), turbidity, conductivity-temperature-depth (CTD), and benthic calcifiers' total species biomass (TSB), performed a Markov chain Monte Carlo simulation of different water sources using salinity and $\delta^{18}\text{O}$, and assessed

¹University of Alaska Fairbanks, International Arctic Research Center, Akasofu Building, Fairbanks, Alaska 99775-7320, USA. ²Tomsk Polytechnic University, 30 Prospect Lenina, 634050 Tomsk, Russia. ³Russian Academy of Sciences, Pacific Oceanological Institute, 43 Baltiiskaya Street, 690041 Vladivostok, Russia. ⁴Stockholm University, Department of Environmental Science and Analytical Chemistry, and the Bolin Centre for Climate Research, 10691 Stockholm, Sweden. ⁵University of Gothenburg, Department of Marine Sciences, 40530 Göteborg, Sweden. ⁶Russian Academy of Sciences, Institute of Chemistry, 159, 100-Let Vladivostok Prospect, 690022 Vladivostok, Russia. ⁷Tiksi Hydrometeorological Service, Tiksi, Yakutia (Sakha) 678400, Russia. *e-mail: igorsm@iarc.uaf.edu

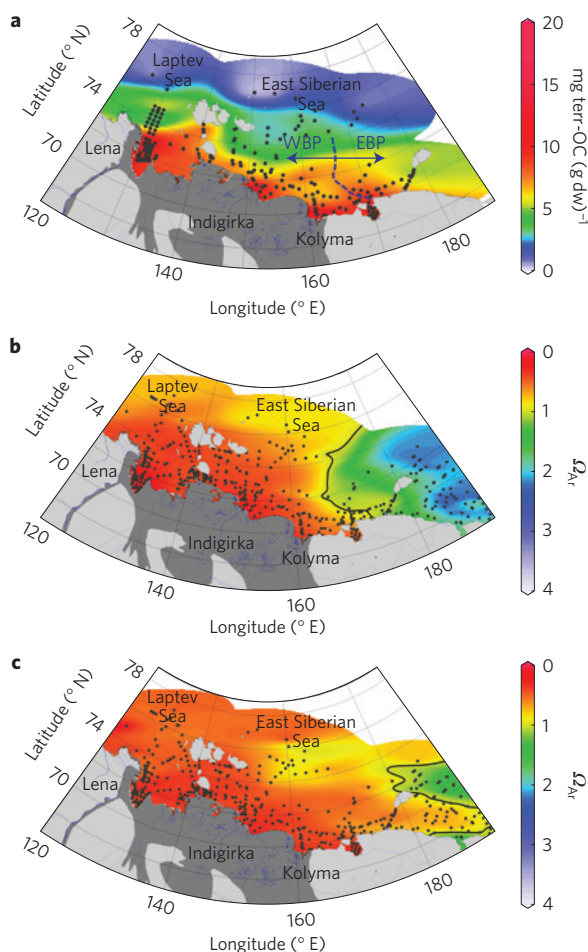


Figure 1 | Spatial distribution on the ESAS system of terr-OC in surface sediments and Ω_{Ar} in the water column. **a, Distribution of terr-OC ($\text{mg terr-OC (g dw)}^{-1}$) in surface sediments over the ESAS as estimated from $\delta^{13}\text{C}$ and OC measurements. **b,c**, Distribution of Ω_{Ar} over the ESAS based on observations over the last 13 years (1999–2011) in surface waters (**b**) and bottom waters (**c**). Black curved lines in **b** and **c** show the position of the boundary along which the Ω_{Ar} equals 1. The blue dotted curve in **a** shows the boundary between two biogeochemical provinces—WBP and EBP.**

DIC concentrations and $\delta^{13}\text{C}_{\text{DIC}}$ compositions in the samples as compared to conservative mixing between river water and sea water. The warmer and fresher Western Biogeochemical Province water (WBP, located eastwards of the Lena Delta to $\sim 160\text{--}170^\circ\text{E}$) is characterized by strong river and coastal erosion impacts (Fig. 1a). The saltier and colder Eastern Biogeochemical Province water (EBP, located eastwards of $\sim 160\text{--}170^\circ\text{E}$) is mainly affected by nutrient-rich Pacific water that creates favourable conditions for high summer primary production³⁰. An extensive data set (>1,500 samples) was collected in years 1999, 2000–2005, 2008 and 2011 (Methods, Supplementary Tables 1 and 2).

The lowest Ω_{Ar} levels were observed in the WBP, where the influence of both river runoff and terr-OC input is much stronger than in the EBP. In the WBP, Ω_{Ar} varied from 0.01 to 1.42 (mean = 0.45, s.d. = 0.23) in surface water (above the pycnocline) (Fig. 1b) and from 0.01 to 1.27 (mean = 0.44, s.d. = 0.23) in bottom water (below the pycnocline) (Fig. 1c). Lower Ω_{Ar} in the WBP was associated with higher p_{CO_2} and lower pH in both surface and bottom water (Supplementary Fig. 2). In bottom water, the decrease in O_2 saturation (<40%) was accompanied by a decrease in pH ($r = 0.79$, $n = 316$, $p < 0.05$) and increase in DIC ($r = -0.59$, $n = 316$, $p < 0.05$); there was a strong correlation between pH and AOU

($r = -0.97$, $n = 108$, $p < 0.05$), suggesting *in situ* organic matter (OM) mineralization, which was manifested in p_{CO_2} buildup and decreasing Ω_{Ar} (Supplementary Table 2 and Supplementary Figs 3 and 4). Most of the surface water was supersaturated with respect to CO_2 ($463.7 \pm 194.2 \mu\text{atm}$, $n = 336$); low pH correlated with high p_{CO_2} ($r = -0.72$, $n = 339$, $p < 0.05$), but correlation between p_{CO_2} and O_2 was weak ($r = -0.44$, $n = 339$, $p < 0.05$). Hence, primary production had a weaker impact on p_{CO_2} than degradation of organic matter. Consequently, there is a need for a source of p_{CO_2} to the WBP surface water. We suggest this is river-transported p_{CO_2} .

Comparison between the observational data and the conservative mixing line for DIC and $\delta^{13}\text{C}_{\text{DIC}}$ revealed that many of the samples in the analysed data set did not fall on the line of conservative mixing between the Lena River water and Arctic sea water (Fig. 2). The most pronounced features were DIC concentrations that fell above the conservative mixing line, and $\delta^{13}\text{C}$ values that were lighter than those expected from conservative mixing; that was consistent with terr-OC degradation, and suggested only a minor role of primary productivity (PP). In the near-shore WBP water, PP was shown to be suppressed by lack of sunlight owing to low transparency of shelf water overloaded with SPM and river-borne CDOM (Supplementary Table 1 and Supplementary Fig. 3). Indeed, our data showed that mean concentrations (\pm s.d.) of SPM and CDOM in the WBP surface water were $12.8 \pm 26.6 \text{ mg l}^{-1}$ and $25.6 \pm 19.1 \mu\text{g l}^{-1}$, respectively; that is, up to ten times greater than in the EBP surface water. In some WBP areas, mean SPM concentrations increased by a factor of 3–5 times during the observed period (Supplementary Fig. 5).

EBP Ω_{Ar} varied from 0.45 to 3.28 (mean = 1.74, s.d. = 0.68) in surface water and from 0.35 to 2.21 (mean = 0.88, s.d. = 0.42) in bottom water. Lower Ω_{Ar} was associated with deeper, saltier, lower-pH water (Supplementary Fig. 2e–h). Correlation between pH and O_2 ($r = 0.75$, $n = 121$, $p < 0.05$) and between DIC and O_2 ($r = -0.64$, $n = 121$, $p < 0.05$) in bottom water clearly points to OC decomposition processes in the water column and water/sediment interface. In surface water, higher pH correlated with lower p_{CO_2} ($r = -0.85$, $n = 121$, $p < 0.05$), as is expected from PP. At the same time, there was no correlation between O_2 and p_{CO_2} ; this could be due to the different air–sea exchange rates of these two gases. Correlation between Ω_{Ar} and salinity ($r = 0.76$, $n = 121$, $p < 0.05$) could be due to seawater freshening. Analysis of multi-year data (1999–2002 versus 2008–2011) revealed a notable trend ($t(331) = 12.77$, $p < 0.05$) towards lower surface water Ω_{Ar} (Supplementary Fig. 6). We attributed this shift to an increasing influence of the riverine plume, which has been propagating further east with the Siberian coastal current over the past ten years (Fig. 3).

To assess the contribution of freshening sources to the Ω_{Ar} state in both biogeochemical provinces, we performed a Markov chain Monte Carlo mass-balance mixing calculation using salinity and $\delta^{18}\text{O}$. Results of the analysis suggest that the mean (± 1 s.d.) contributions of three endmembers (sea water, riverine water, and ice melt water) to the surface water compose $59.7 \pm 4\%$, $34.3 \pm 3.5\%$, and $5.9 \pm 4\%$ in the WBP and $87.5 \pm 5.4\%$, $5 \pm 2.8\%$, and $7.4 \pm 5\%$ in the EBP, respectively (Fig. 4). The WBP surface water Ω_{Ar} reflects the freshening effect of river discharge, which also adds water with river-transported p_{CO_2} and translocated terr-OC, some of which gets degraded to CO_2 in the recipient shelf water, resulting in significantly decreased Ω_{Ar} , >3.5 times lower in the WBP than in the EBP (0.45 versus 1.74, $t(141) = 20.91$, $p < 0.05$). Ω_{Ar} in EBP surface water varied from 0.45 to 3.28, but averaged slightly above 1, possibly reflecting the interplay between the rivers' freshening effect and CO_2 removal during photosynthesis supported by nutrient-rich Pacific-derived waters^{27,30}.

To investigate the role of the river-freshening effect versus terr-OC input due to coastal erosion, we established two groups of WBP sites where the contribution from each source was expected

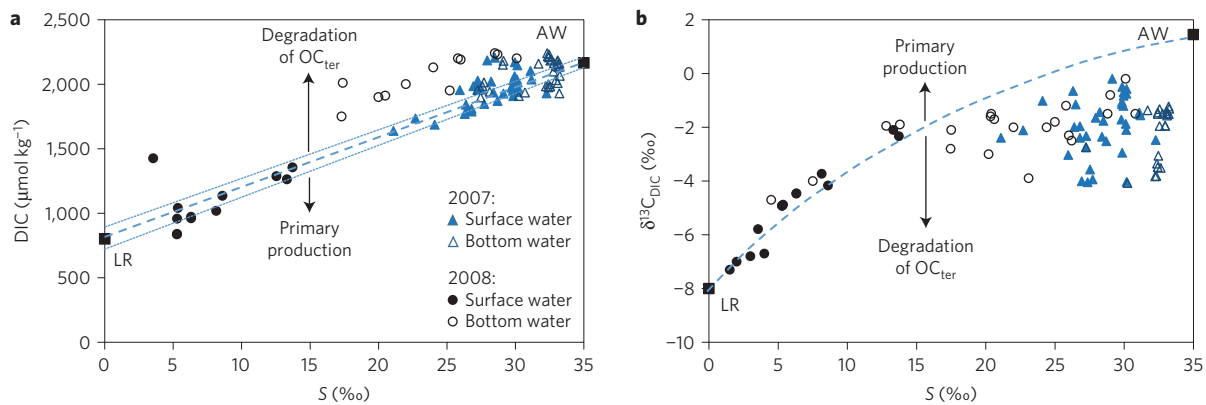


Figure 2 | Calculated two-component mixing lines between two endmembers: the Arctic water (AW) and Lena River water (LR). **a**, DIC plotted against salinity. **b**, $\delta^{13}\text{C}$ plotted against salinity. For **a** and **b** the endmembers and details of the method used can be found in ref. 27; AW – DIC = $2,200 \pm 2\%$ μM $\delta^{13}\text{C} = 1.45\%$; LR – DIC = $810 \pm 79\%$ μM (mean \pm 95% confidence interval (CFI 95%) marked by the dashed line), $\delta^{13}\text{C} = -8\%$. Original data collected by authors in 2007 are combined with data from ref. 27.

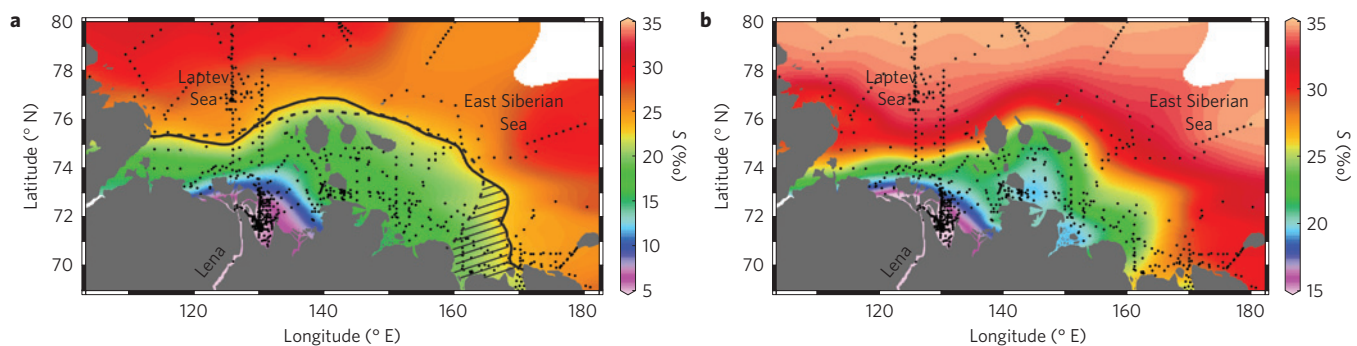


Figure 3 | Distribution of salinity (‰) in the EBP inferred from multi-year data. **a**, **b**, Summertime salinity observed in 2000–2012 versus that observed in 1932–2000 in surface water (**a**) and in bottom water (**b**). In **a** the position of the isohaline = 23% observed in 2000–2012 is marked as a black solid line (2000–2012); its position in 1932–2000 is marked as a black dotted line; the area of its extension to the east during the last 12 years, equal to $\sim 116,000\text{ km}^2$, is shown as the hatched area.

to be high: the Lena River estuary (large freshening effect, five stations), and an area near the coast that was exhibiting high coastal erosion rates (large eroded terr-OC impact, three stations). We also investigated two groups of control sites: one group in the Lena River delta (10 stations) and one group of offshore sites away from the direct influence of either river discharge or coastal erosion (28 stations, Supplementary Fig. 1d). Our results show that the acidifying effect of terr-OC decomposition at the erosion-dominated site was more than five times stronger than that of estuary freshening (531% versus 100.5%), (Supplementary Table 3). Inter-annual variability in DIC (Supplementary Fig. 3b) and Ω_{Ar} (Supplementary Fig. 7) could be attributed to dynamics in coastal erosion rates²¹ and to the hydraulic regime of the Arctic rivers (Supplementary Fig. 8).

We suggest that low Ω_{Ar} observed in the bottom water in both ESAS biogeochemical provinces is determined by *in situ* OC decomposition. Because rates of coastal erosion and the acidifying effect of terr-OC input due to coastal erosion and river input are higher in the WBP than in the EBP^{21,26}, this results in mean WBP Ω_{Ar} that is half as much as in the EBP [0.44 versus 0.88, $t(158) = 12.35$, $P < 0.054$]. Because shelf water with $\Omega_{\text{Ar}} < 1$ is corrosive, it might cause dissolution of the CaCO_3 that forms the benthic species' shells and skeletons. Long-term effects of lower Ω_{Ar} could result in lower biomass of benthic calcifying species and further suppression of their populations. Indeed, we observed that the TSB of WBP macro-benthic calcifying species varies by a factor of five, with the lowest TSB values observed where $p\text{CO}_2$ was highest

and Ω_{Ar} was lowest (Supplementary Fig. 9). This distribution in the benthic calcifying community could be a direct consequence of seawater acidification.

The results of this study clearly show a major OA pattern in the ESAS resulting in severe Ar undersaturation of shelf waters caused by degradation of terr-OC exported from thawing coastal permafrost, and freshening due to growing Arctic river runoff from extensive permafrost-underlain watersheds and ice melt. In contrast to other marine ecosystems, where organic carbon originates from planktonic and riverine sources, coastal erosion represents a significant source of terr-OC to the ESAS. The dual-carbon isotope ($\delta^{13}\text{C}$ and ^{14}C) composition of ESAS OC establishes that old permafrost-released erosional carbon dominates burial of OC on the ESAS, and that $57 \pm 2\%$ of this terr-OC is from permafrost-originated ice complexes of Pleistocene age²³. This translocated terr-OC represents a source of OA different from that of the generally considered atmospheric CO_2 uptake. Persistent and potentially increasing Ar undersaturation of ESAS water has already far exceeded projected levels for the year 2100, which are based only on atmospheric CO_2 uptake (Supplementary Fig. 10). Because Ar undersaturation is characteristic of the entire ESAS bottom water, we suggest that the observed suppression of the benthic calcifying community might be pervasive throughout the entire ESAS, which alone composes $>25\%$ of the Arctic Ocean open water. As these waters are exported to the surface of the central Arctic Ocean by the transpolar drift as well as into the Beaufort Gyre, the consequences of OA, triggered by climate-change-driven mechanisms, might

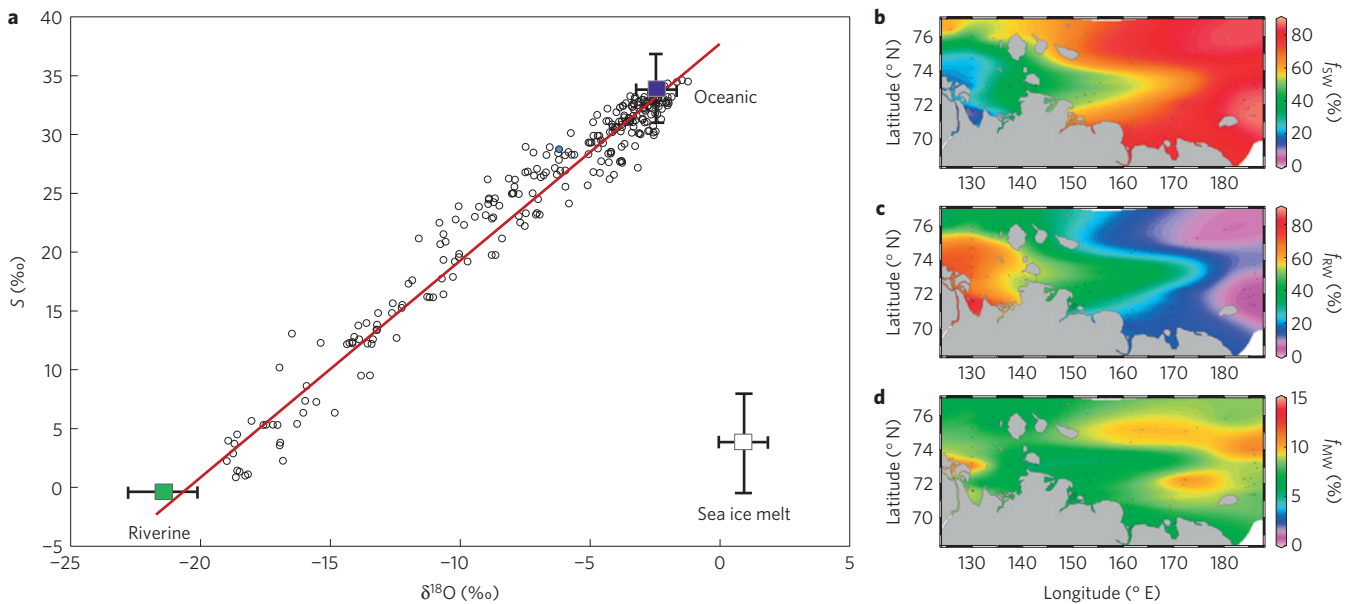


Figure 4 | A two-dimensional source marker ($\delta^{18}\text{O}$ versus salinity) plot. **a, Black circles represent individual data points, whereas the endmember ranges (mean \pm s.d.) for the three main sources: oceanic (blue), riverine (green) and sea ice melt (white) are represented with error bars. The red line represents a linear fit of the individual data points ($R^2 = 0.96$), suggesting overall minor sea ice melt contributions and good agreement between the oceanic and riverine endmember values and the data. **b–d**, Geographically resolved estimated relative (%) source contributions from oceans (**b**), rivers (**c**) and sea ice melt (**d**).**

affect Arctic marine ecosystems over extensive scales. This study also calls into question the capacity of the Arctic Ocean to serve as a sink for a growing amount of anthropogenic CO_2 .

Methods

Methods and any associated references are available in the [online version of the paper](#).

Received 2 September 2015; accepted 9 March 2016;
published online 18 April 2016; corrected after print 6 May 2016

References

- Arctic Climate Impact Assessment (ACIA) *Impacts of a Warming Arctic* Ch. 4, 99–150 (Cambridge Univ. Press, 2005).
- Orr, J. C. *et al.* Anthropogenic ocean acidification over the twenty-first century and its impact on calcifying organisms. *Nature* **437**, 681–686 (2005).
- Hoegh-Guldberg, O. & Bruno, J. F. The impact of climate change on the world's marine ecosystems. *Science* **328**, 1523–1528 (2010).
- Arctic Monitoring and Assessment Programme (AMAP) *AMAP Assessment 2013: Arctic Ocean Acidification* (Narayana Press, 2013).
- Bates, N. R., Mathis, J. T. & Cooper, L. W. Ocean acidification and biologically induced seasonality of carbonate mineral saturation states in the western Arctic Ocean. *J. Geophys. Res.* **114**, C11007 (2009).
- Guinotte, J. M. & Fabry, V. J. Ocean acidification and its potential effects on marine ecosystems. *Ann. N. Y. Acad. Sci.* **1134**, 320–342 (2008).
- Mucci, A. The solubility of calcite and aragonite in seawater at various salinities, temperatures, and one atmosphere total pressure. *Am. J. Sci.* **283**, 780–799 (1983).
- Doney, S. C., Fabry, V. J., Feely, R. A. & Kleypas, J. A. Ocean acidification: the other CO_2 problem. *Annu. Rev. Mar. Sci.* **1**, 169–192 (2009).
- Yamamoto-Kawai, M., McLaughlin, F. A., Carmack, E. C., Nishino, S. & Shimada, K. Aragonite undersaturation in the Arctic Ocean: effects of ocean acidification and sea ice melt. *Science* **326**, 1098–1100 (2009).
- Steinacher, M., Joos, F., Frolicher, T. L., Plattner, G.-K. & Doney, S. C. Imminent ocean acidification in the Arctic projected with the NCAR global coupled carbon cycle-climate model. *Biogeosciences* **6**, 515–533 (2009).
- Bianchi, T. S. *et al.* Enhanced transfer of terrestrially derived carbon to the atmosphere in a flooding effect. *Geophys. Res. Lett.* **40**, 116–122 (2013).
- Semiletov, I. P. *et al.* Space-time dynamics of carbon and environmental parameters related to carbon dioxide emissions in the Buor-Khaya Bay and adjacent part of the Laptev Sea. *Biogeosciences* **10**, 5977–5996 (2013).
- Vonk, J. E. & Gustafsson, Ö. Permafrost-carbon complexities. *Nature Geosci.* **6**, 675–676 (2013).
- Peterson, B. J. *et al.* Increasing river discharge to the Arctic Ocean. *Science* **298**, 2171–2173 (2002).
- Savelieva, N. I., Semiletov, I. P., Vasilevskaya, L. N. & Pugach, S. P. A climate shift in seasonal values of meteorological and hydrological parameters for northeastern Asia. *Prog. Oceanogr.* **47**, 279–297 (2000).
- Shakhova, N. *et al.* Ebullition and storm-induced methane release from the East Siberian Arctic Shelf. *Nature Geosci.* **7**, 64–70 (2014).
- Semiletov, I. P., Shakhova, N. E., Sergienko, V. I., Pipko, I. I. & Dudarev, O. V. On carbon transport and fate in the East Siberian Arctic land-shelf-atmosphere system. *Environ. Res. Lett.* **7**, 015101 (2012).
- Semiletov, I. P. *et al.* Carbon transport by the Lena River from its headwaters to the Arctic Ocean, with emphasis on fluvial input of terrestrial particulate organic carbon vs. carbon transport by coastal erosion. *Biogeosciences* **8**, 2093–2143 (2011).
- Romanovskii, N. N., Hubberten, H.-W., Gavrillov, A., Eliseeva, A. & Walker, D. Offshore permafrost and gas hydrate stability zone on the shelf of East Siberian seas. *Geo-Mar. Lett.* **25**, 167–182 (2005).
- Charkin, A. N. *et al.* Seasonal and interannual variability of sedimentation and organic matter distribution in the Buor-Khaya Gulf: the primary recipient of input from Lena River and coastal erosion in the southeast Laptev Sea. *Biogeosciences* **8**, 2581–2941 (2011).
- Günther, F., Overduin, P. P., Sandakov, A. V., Grosse, G. & Grigoriev, M. N. Short- and long-term thermo-erosion of ice-rich permafrost coasts in the Laptev Sea region. *Biogeosciences* **10**, 4297–4318 (2013).
- Gustafsson, Ö., van Dongen, B. E., Vonk, J. E., Dudarev, O. V. & Semiletov, I. P. Widespread release of old carbon across the Siberian Arctic echoed by its large rivers. *Biogeosciences* **8**, 1737–1743 (2011).
- Vonk, J. E. *et al.* Activation of old carbon by erosion of coastal and subsea permafrost in Arctic Siberia. *Nature* **489**, 137–140 (2012).
- Pipko, I. I., Semiletov, I. P., Tishchenko, P. Ya., Pugach, S. P. & Savelieva, N. I. Variability of the carbonate system parameters in the coast-shelf zone of the East Siberian Sea during the autumn season. *Oceanologiya* **48**, 54–67 (2008).
- Anderson, L. G., Jutterström, S., Hjalmarsson, S., Wahlström, I. & Semiletov, I. P. Fluxes and transformation of carbon in the Siberian shelf seas under changing environment. *Geophys. Res. Lett.* **36**, L20601 (2009).
- Pipko, I. I., Semiletov, I. P., Pugach, S. P., Wahlstrom, I. & Anderson, L. G. Interannual variability of air-sea CO_2 fluxes and carbon system in the East Siberian Sea. *Biogeosciences* **8**, 1987–2007 (2011).
- Alling, V. *et al.* Degradation of terrestrial organic carbon, primary production and out-gassing of CO_2 in the Laptev and East Siberian seas as inferred from $\delta^{13}\text{C}$ values of DIC. *Geochim. Cosmochim. Acta* **95**, 143–159 (2012).

28. Sánchez-García, L. *et al.* Distribution, sources and inventories of particulate organic carbon in the Laptev and East Siberian seas. *Glob. Biogeochem. Cycles* **25**, GB2007 (2011).
29. Semiletov, I. *et al.* The East Siberian Sea as a transition zone between Pacific-derived waters and Arctic shelf waters. *Geophys. Res. Lett.* **32**, L10614 (2005).
30. Anderson, L. G. *et al.* East Siberian Sea, an Arctic region of very high biogeochemical activity. *Biogeosciences* **8**, 1745–1754 (2011).

Acknowledgements

This research was supported by the Russian Government (No. 14.Z50.31.0012/03.19.2014); the Russian Foundation for Basic Research (Nos. 13-05-12028, 13-05-12041, 13-05-12042, 14-05-00433); the Headquarters of the Russian Academy of Sciences, RAS (Arctic Program led by A. Khanchuk), the Far Eastern Branch of RAS; the US National Science Foundation (OPP ARC-1023281; 0909546); the NOAA Climate Program office (NA08OAR4600758); the Swedish Knut and Alice Wallenberg Foundation (KAW); the Swedish Research Council (VR); and the Nordic Council of Ministers (NMR-TRI-Defrost). N.S., A.C. and O.D. acknowledge support from the Russian Science

Foundation (No. 15-17-20032). I.S. and N.S. also acknowledge ICE-ARC-EU FP7 project. We thank C. O'Connor for English editing.

Author contributions

I.S., I.P., O.G. and L.G.A. designed the fieldwork; I.P., S.P., O.D. and A.C. set up the analytical instruments, performed the on-board measurements, collected the data, and conducted quality control; A.G. collected and analysed macro-benthos data; I.P., S.P., L.B., A.A. and E.S. designed the figures; I.S., N.S. and O.G. drafted the first manuscript; and all authors contributed to the final version.

Additional information

Supplementary information is available in the [online version of the paper](#). Reprints and permissions information is available online at www.nature.com/reprints. Correspondence and requests for materials should be addressed to I.S.

Competing financial interests

The authors declare no competing financial interests.

Methods

Data gathering. Seawater samples were collected in Niskin bottles and then transferred into smaller bottles for chemical analysis. pH was determined potentiometrically and reported on the total hydrogen ion concentration scale³¹. pH measurement precision was about ± 0.004 pH units. Direct comparison between potentiometric and spectrophotometric pH measurements (both on the 'total' scale) was carried out in September 2008. Results of this comparison demonstrate good concurrence between the two methods³². In 2008, the carbon dioxide (CO₂) system was studied by measuring concentrations of dissolved inorganic carbon (DIC), total alkalinity (TA) and pH, and computations using the different constituents showed good pH accuracy; DIC and TA were calibrated versus certified reference materials (CRMs) supplied by A. Dickson, Scripps Institution of Oceanography.

TA. In August–September 2004 and 2005, and in winter 2002 and 2007, TA was determined as proposed in DOE³¹. The TA samples were poisoned with a mercuric chloride solution at the time of sampling. Samples were kept in the dark and were analysed in the lab within one month using an indicator titration method in which 25 ml of sea water was titrated with 0.02 M hydrochloric acid (HCl) in an open cell according to Bruevich³³. In 2000 the Carbon Dioxide in the Ocean working group of the North Pacific Marine Science Organization (PICES) performed an intercalibration of TA in sea water using CRMs. The results of the intercalibration showed that the alkalinity values obtained by the Bruevich method are in agreement with the standard within $\pm 1 \mu\text{mol kg}^{-1}$ when state-of-the-art analytical practice is applied³⁴. In August–September 2008, TA was determined after pH from the same sample on board the 'Yakob Smirnitkiy', using an open-cell potentiometric titration method; 0.05 M HCl was used and the end point was determined by a Gran function³⁵. The concentrations thus obtained were calibrated against CRMs. In September 2011, A_T was determined on board the 'Academic Lavrentiev' according to Bruevich³³, again using CRMs. The precision of both titration methods was similar, at about 0.1%.

DIC. To measure DIC (fall seasons in 1999, 2000) we used a TS-VET-530 or LKHM-80MD gas chromatograph (GC), with a Poropak T (1.5 m, 80–120 mesh) and a flame-ionization detector (FID) run isothermally at 30 °C with hydrogen carrier gas; a stripping GC technique similar to that described in Weiss³⁶ was used. The total CO₂ (TCO₂) calibrations were based on 0.73, 1.02 and 1.99 mM standard solutions of sodium carbonate (Na₂CO₃) that were prepared gravimetrically in freshly distilled water. Conversion of CO₂ to methane (CH₄) after the Poropak column was done in a nickel (Ni)-catalyst column (14 cm Chromaton, 80–100 mesh, coated with Ni) at 400 °C (ref. 37). The measurements are reproducible to within ± 1 –2%. In August–September 2008, DIC was determined by a coulometric titration method³¹, having a precision of ~ 2 mmol kg⁻¹, with the accuracy set by calibration against certified reference materials (CRM), supplied by A. Dickson, Scripps Institution of Oceanography (USA). The seawater DIC was computed from pH–TA using CO₂SYS³⁸ for cruises in 2003, 2004, 2005, 2007 and 2011.

Partial pressure of CO₂ (p_{CO₂}). The seawater p_{CO₂} was computed from pH–TA using CO₂SYS³⁸, except for cruises in 1999 and 2000, during which the pH–C_T pair was used. The carbonic acid dissociation constants (K₁ and K₂) of Mehrbach *et al.*³⁹, as refitted by Dickson and Millero⁴⁰, were used. The uncertainty in computed p_{CO₂} was about $\pm 10 \mu\text{atm}$.

Dissolved oxygen (O₂), Ω_{O₂} and apparent oxygen utilization (AOU).

O₂ concentrations were obtained using a Winkler titration system, giving a precision of $\sim 3 \mu\text{mol kg}^{-1}$ for 1999–2005 data and $\sim 1 \mu\text{mol kg}^{-1}$ for 2008 and 2011 data. These values were then converted to percentage saturation (Ω_{O₂}), following Weiss³⁶. AO_U represents one estimate of the O₂ utilized due to biochemical processes relative to a preformed value. AO_U was calculated as the difference between the O₂ gas solubility ([O₂^{*}]) and the measured O₂ concentrations, expressed as AO_U = [O₂^{*}] – [O₂], in which O₂^{*} is the O₂ solubility concentration calculated as a function of *in situ* temperature and salinity, and one atmosphere of total pressure⁴¹.

Nutrients. Nitrates, nitrites, silicates and phosphates were determined by traditional oceanographic techniques prescribed in ref. 42. In September 2008, nutrients were determined using a SmartChem analyser (Westco Scientific Instruments; <http://www.westcoscientific.com/pages/smartchem200.htm#applications>). More detailed descriptions can be found elsewhere^{43,44}. The samples were filtered before analysis and evaluated by a 6- to 8-point calibration curve at $\sim 1\%$ precision.

Dissolved organic carbon (DOC). DOC contents of samples sealed in glass tubes were determined using a Shimadzu TOC-5000 high-temperature catalytic oxidation technique in the University of Alaska Fairbanks laboratories.

Hydrological parameters. During the 2004–2011 cruises, a Seabird SBE19plus Profiler (www.seabird.com) was used for measurements of conductivity,

temperature, photosynthetically active radiation (PAR) (by LI-193SA Spherical Quantum Sensor), turbidity (by OBS-3 Sensor) and fluorescence. A WetStar fluorimeter was used to assess the *in situ* coloured dissolved organic matter (CDOM) concentration; this instrument has a single excitation (E_x = 370 nm)/emission (E_m = 460 nm) wavelength pair. These measurements characterized the distribution of CDOM at vertical intervals of 0.20 m at the oceanographic stations.

Total species biomass (TSB). Samples were collected using a Van-Veen grab (0.1 m²) and a Petersen grab with a sampling area of 0.025 m² to a depth of 10 cm. Samples were gently sieved through 0.5 mm mesh screen using ambient sea water. The material retained on the screen was transferred to 1-l labelled glass jars and preserved in sea water with 10% buffered formalin and Rose Bengal stain. In the laboratory, samples were washed in fresh water; the organisms were separated from the detritus and sorted into major taxa using a binocular dissecting microscope. After sorting, the organisms were weighed (accuracy ± 0.001 g), fixed by 70% ethanol, identified to the lowest possible taxonomic level (species), and counted. Ash-free dry weight biomass was measured for each species by drying the organisms to a constant weight at 60 °C, followed by ashing in a muffle furnace at 500 °C for four hours. TSB was calculated as ash-free dry weight, summed over all the organisms in the sample, and normalized to grams per metre squared of the sea floor^{45–47}.

Saturation level of aragonite (Ω_{Ar}). Ω_{Ar} was also computed from pH and A_T using the same software, CO₂SYS, and constants. Calcium carbonate (CaCO₃) Ω of the waters was calculated as: Ω = [Ca²⁺] · [CO₃²⁻]/K_{sp}, where [Ca²⁺] and [CO₃²⁻] are the concentrations of dissolved calcium and carbonate ions respectively, and K_{sp} is the apparent solubility product, which depends on temperature, salinity, pressure, and the particular mineral phase⁴⁸.

Terrestrial organic carbon (terr-OC). Terr-OC concentrations were derived from δ¹³C and OC measurements. Source apportionment calculations were performed with a marine endmember δ¹³C signature of –24‰ for the WBP and –21‰ for the EBP. These values were chosen based on previous studies^{49–52}. For the terrigenous endmember, the weighted average δ¹³C of ice-complex deposits (80%, δ¹³C = –32.1‰, ref. 51) and topsoil permafrost sources (20%, δ¹³C = –26.3‰, ref. 51) was used (δ¹³C_{terr} = –27.5‰). Results of the mass-balance equations were then multiplied by measured OC concentrations for every location.

Suspended particulate material (SPM). The SPM content was obtained by filtration through membrane filters with a pore diameter of 0.47 μm followed by gravimetry; the details can be found elsewhere⁵³.

Water source apportionment. The relative contributions of riverine, sea melt, and Arctic Ocean to collected water samples were differentiated using salinity and the stable oxygen isotope signature (δ¹⁸O) as source markers in a mass-balance mixing model⁵⁴. The endmember values for the three sources were estimated as: riverine, salinity 0 psu, δ¹⁸O –21.4 ± 1.7‰; sea melt, salinity 4 ± 4 psu, δ¹⁸O 1 ± 1‰; Arctic Ocean, salinity 33.3 ± 2.9 psu, δ¹⁸O –2.5 ± 1‰ (refs 55–57). To account for the variability in the endmember values, the mean fractional contribution of the three sources for each sampling station was estimated using a Markov chain Monte Carlo approach⁵⁸. For each sampling station, the mean source signature of multiple water samples was used for the source apportionment calculations.

Assessment of the shift in acidity. Ocean acidification refers to a reduction on the pH of the sea water over an extended period. pH is measured by concentration of hydrogen ions (H⁺ or [H⁺]) in a solution that is expressed on a log scale ranging from 0 to 14 (equals to 1 to 10^{–14} moles per litre), where pH is defined as minus the logarithm of [H⁺] (that is, pH = –log₁₀[H⁺]). Thus, a tenfold change in the hydrogen ion concentration results in a pH change of 1. Ocean acidification (OA) is attributed to the increased concentrations of CO₂, which combined with water forms carbonic acid (H₂CO₃), a weak acid, which then partially dissociates to release H⁺ ions that lead to increasing acidity of the ocean. As p_{CO₂} of the sea water increases, the acidity increases and pH decreases. The change in acidity observed at four groups of sites presented in the Supplementary Table 3 was assessed following ref. 4, which are sourced from the National Oceanic and Atmospheric Administration (NOAA) Pacific Marine Environmental Laboratory (PMEL). According to this source, shift in pH = 8.2 (that is, H⁺ = 6.3 × 10^{–9}) to pH = 8.1 (that is, H⁺ = 7.9 × 10^{–9}), equal to a change in acidity of +26%; shift in pH = 8.2 (that is, H⁺ = 6.3 × 10^{–9}) to pH = 7.9 (that is, H⁺ = 1.3 × 10^{–8}) equal to a change in acidity of +100% and so on. The reference level was set based on the mean global pH of 8.2 at the beginning of the Industrial Revolution⁴.

Measurements of δ¹⁸O and δ¹³C_{DIC}. δ¹⁸O values were determined using a Thermal Conversion Elemental Analyzer (TC/EA) and a Finigan Delta V spectrometer at Stockholm University, Department of Geological Sciences. Stable isotope ratios were reported in notation as parts per thousand (‰) deviation from the international standards, V-SMOW (Vienna Standard Mean Ocean Water). The

overall precision based on standard measurements is estimated to be better than 0.1‰ (ref. 60). For the determination of C isotope composition in water, we followed similar sampling techniques to those described in ref. 59. $\delta^{13}\text{C}$ of DIC values are measured using a Thermo GasBench II carbonate analyser with a DeltaPlusXP Mass Spectrometer at the Institute of Marine Sciences/University Alaska Fairbanks Isotope Facilities. Water samples use 1 to 0.5 ml, and are placed into square bottom exetainer tubes. The tubes are purged for 20 min with ultra purified helium and then 0.1 ml of 85% H_3PO_4 is manually added by syringe to the sample through the septum. The headspace gases are then transferred to the GasBench II, where the water is removed through a Nafion dryer. CO_2 is separated chromatographically from other gases present, and then transferred to the IRMS, where the isotopes of carbon are measured. $\delta^{13}\text{C}_{\text{PDB}}$ values are reported with reference to international isotope standards. The quality control scheme involves analysing a blank every twenty samples and two laboratory working standards every ten samples. Twice a year, the laboratory working standards are compared to NIST and IAEA standards to confirm quality assurance.

Estimation of population parameters. Variables from each data set were plotted as different distributions in the Minitab 17 statistics software package and were tested using the Goodness of Fit Test⁶¹. The test for normality was performed via the Anderson Darling test, for which the null hypothesis (H_0) is that data are normally distributed and the alternative hypothesis (H_A) is that data are not normally distributed. Because both subpopulations have a p value above 0.05, it was concluded that variances in both subpopulations are normally distributed. Descriptive statistics for normal distribution were calculated as arithmetic mean (M) \pm 1 standard deviation (s.d.). To compare whether the average difference between two subpopulations (M) (the Western Biogeochemical Province, WBP, and the Eastern Biogeochemical Province, EBP) is significant, or if it is due to random chance, we applied the two-sample t -test using Minitab 17 statistics software. H_0 stated that the difference between two means ($M_1 - M_2$) equals zero; H_A stated that the difference is not equal to zero. Data were standardized; standard errors (SEs) of M and t -values were calculated. The method was applicable to all subpopulations because they were all greater than 30 samples. Alpha (α) was set at 0.05. The critical value of standardized difference of the $M(t)$ s was set at 2.06. The difference between subpopulations was determined to be significant if the t -value was larger than 2.06. Results of independent group t -tests in the main text and Supplementary Tables 5–7 are presented as subpopulation mean, s.d. and SE of the mean, t -value with degree of freedom (DF), and p value.

References

- Dickson, A. G. & Goyet, C. (eds) *Handbook of Methods for the Analysis of the Various Parameters of the Carbon Dioxide System in Seawater* Version 2, ORNL/CDIAC-74 (DOE, 1994).
- Pipko, I. I., Semiletov, I. P., Pugach, S. P., Wahlstrom, I. & Anderson, L. G. Interannual variability of air-sea CO_2 fluxes and carbon system in the East Siberian Sea. *Biogeosciences* **8**, 1987–2007 (2011).
- Bruevich, S. V. *Instruction for Chemical Investigation of Seawater* Vol. 83 (Glavsevmorput, 1944).
- Pavlova, G. Y., Tishchenko, P. Y., Volkova, T. I., Dickson, A. & Wallmann, K. Intercalibration of Bruevich's method to determine the total alkalinity in seawater. *Oceanologia* **48**, 23–32 (2008).
- Haraldsson, C., Anderson, L. G., Hasselov, M., Hulth, S. & Olsson, K. Rapid, high-precision potentiometric titration of alkalinity in ocean and sediment pore waters. *Deep-Sea Res. I* **44**, 2031–2044 (1997).
- Weiss, R. F. Determinations of carbon dioxide and methane by dual catalyst flame ionization chromatography and nitrous oxide by electron capture chromatography. *J. Chromatogr. Sci.* **19**, 611–616 (1981).
- Semiletov, I. P. in *Ancient Ice Air Content of the Vostok Ice Core: Biogeochemistry of Trace Gases* (ed. Oremland, S.) 46–59 (Chapman and Hall, 1993).
- Lewis, E. & Wallace, D. W. R. *Program Developed for CO_2 System Calculations* ORNL/CDIAC-105 (Carbon Dioxide Information Analysis Center, Oak Ridge National Laboratory, 1998).
- Mehrbach, C., Culbertson, C. H., Hawley, J. E. & Pytkowicz, R. M. Measurement of the apparent dissociation constants of carbonic acid in seawater at atmospheric pressure. *Limnol. Oceanogr.* **18**, 897–907 (1973).
- Dickson, A. G. & Millero, F. J. A comparison of the equilibrium constants for the dissociation of carbonic acid in seawater media. *Deep-Sea Res. A* **34**, 1733–1743 (1987).
- Garcia, H. E., Locarnini, R. A., Boyer, T. P. & Antonov, J. I. *World Ocean Atlas 2005 Volume 3: Dissolved Oxygen, Apparent Oxygen Utilization, and Oxygen Saturation* (ed. Levitus, S.) NOAA Atlas NESDIS, Vol. 63 (Government Printing Office, 2011).
- Ivanenkov, V. N. & Bordovsky, O. K. *Methods of Hydrochemical Investigation of Seawater* [in Russian] (Nauka Press, 1978).
- Anderson, L. G., Jutterström, S., Hjalmarsson, S., Wählström, I. & Semiletov, I. P. Fluxes and transformation of carbon in the Siberian shelf seas under changing environment. *Geophys. Res. Lett.* **36**, L20601 (2009).
- Anderson, L. G. *et al.* East Siberian Sea, an Arctic region of very high biogeochemical activity. *Biogeosciences* **8**, 145–1754 (2011).
- Gukov, A. Yu. Benthic biocenosis in the Buor-Khaya Bay (the Laptev Sea). *Oceanologia* **2**, 316–317 (1989).
- Gukov, A. Yu. Hydrobiological research in the Lena polynya. *Ber. Polarforsch* **176**, 230–232 (1995).
- Rachor, A., Hinz, K. & Sirenko, B. I. Macrofauna. *Ber. Polarforsch* **149**, 97–106 (1994).
- Mucci, A. The solubility of calcite and aragonite in seawater at various salinities, temperatures, and one atmosphere total pressure. *Am. J. Sci.* **283**, 780–799 (1983).
- Semiletov, I. *et al.* The East Siberian Sea as a transition zone between Pacific-derived waters and Arctic shelf waters. *Geophys. Res. Lett.* **32**, L10614 (2005).
- Vonk, J. E. *et al.* Molecular and radiocarbon constraints on sources and degradation of terrestrial organic carbon along the Kolyma paleoriver transect, East Siberian Sea. *Biogeosciences* **7**, 3153–3166 (2010).
- Vonk, J. E. *et al.* Activation of old carbon by erosion of coastal and subsea permafrost in Arctic Siberia. *Nature* **489**, 137–140 (2012).
- Karlsson, E. S. *et al.* Carbon isotopes and lipid biomarker investigation of sources, transport and degradation of terrestrial organic matter in the Buor-Khaya Bay, SE Laptev Sea. *Biogeosciences* **8**, 1865–1879 (2011).
- Charkin, A. *et al.* Seasonal and interannual variability of sedimentation and organic matter distribution in the Buor-Khaya Gulf: the primary recipient of input from Lena River and coastal erosion in the southeast Laptev Sea. *Biogeosciences* **8**, 2581–2941 (2011).
- Anderson, L. G. *et al.* Source and formation of the upper halocline of the Arctic Ocean. *J. Geophys. Res.* **118**, 410–421 (2013).
- Gordeev, V. V., Martin, J. M., Sidorov, I. S. & Sidorova, M. V. A reassessment of the Eurasian river input of water, sediments, major elements, and nutrients to the Arctic Ocean. *Am. J. Sci.* **296**, 664–691 (1996).
- Cooper, L. W. *et al.* Flow-weighted values of runoff tracers (d^{18}O , DOC, Ba, alkalinity) from the six largest Arctic rivers. *Geophys. Res. Lett.* **35**, L18606 (2008).
- Lansard, B. *et al.* Seasonal variability of water mass distribution in the southeastern Beaufort Sea determined by total alkalinity and $\delta^{18}\text{O}$. *J. Geophys. Res.* **117**, C03003 (2012).
- Andersson, A. *et al.* Regionally-varying combustion sources of the January 2013 severe haze events over eastern China. *Environ. Sci. Technol.* **49**, 2038–2043 (2015).
- Alling, V. *et al.* Degradation of terrestrial organic carbon, primary production and out-gassing of CO_2 in the Laptev and East Siberian seas as inferred from $\delta^{13}\text{C}$ values of DIC. *Geochim. Cosmochim. Acta* **95**, 143–159 (2012).
- Rosén, P.-O. *et al.* Ice export from the Laptev and East Siberia Sea derived from $\delta^{18}\text{O}$ values. *J. Geophys. Res.* **120**, 5997–6007 (2015).
- Markowski, C. & Markowski, E. Conditions for the effectiveness of a preliminary test of variance. *Am. Stat.* **44**, 322–326 (1990).

Addendum: Acidification of East Siberian Arctic Shelf waters through addition of freshwater and terrestrial carbon

Igor Semiletov, Irina Pipko, Örjan Gustafsson, Leif G. Anderson, Valentin Sergienko, Svetlana Pugach, Oleg Dudarev, Alexander Charkin, Alexander Gukov, Lisa Bröder, August Andersson, Eduard Spivak and Natalia Shakhova

Nature Geoscience **9**, 361–365 (2016); published online 18 April 2016; addendum published after print 8 August 2016.

In the version of this Letter originally published the data availability statement was not included and it should have read: All seawater data are publicly and freely available at [Bolin Centre Database](#); $\delta^{18}\text{O}$ -data plotted in Fig. 4 are from ref. 60 and are available at the [British Oceanographic Data Centre](#) web site.